Available online at www.sciencedirect.com
ScienceDirect
Journal of Power Sources 173 (2007) 502–509
JOURNAL OF POWER SOURCES
www.elsevier.com/locate/jpowsour

Effect of calcination temperature on morphology, crystallinity and electrochemical properties of nano-crystalline metal oxides (Co_3O_4, CuO, and NiO) prepared via ultrasonic spray pyrolysis

Sung Woo Oh, Hyun Joo Bang, Young Chan Bae, Yang-Kook Sun *

Department of Chemical Engineering, Center for Information and Communication Materials, Hanyang University, Seongdong-Gu, Seoul 133-791, Republic of Korea

Received 16 February 2007; accepted 22 April 2007
Available online 10 May 2007

Abstract

Nano-crystalline metal oxides (Co_3O_4, CuO, and NiO) are synthesized as anode materials for lithium-ion batteries by an ultrasonic spray pyrolysis method. The effects of calcination temperature on the morphology, crystallite size and electrochemical properties of the metal oxides are investigated. X-ray diffraction (XRD) studies show that the crystallite size varies with the final calcination temperature. Scanning electron microscopy (SEM) and transmission electron microscopy (TEM) observations reveal that the calcination temperature strongly influences the morphology of the prepared metal oxides and this results in different electrochemical performance. The existence of a nano-scale microstructure for the prepared metal oxides has a strong relationship with irreversible capacity and capacity retention.

Keywords: Lithium secondary batteries; Spray pyrolysis; Anode material; Electrochemical properties; Nano-crystalline metal oxide; Calcination temperature

1. Introduction

In recent years, intensive research efforts have been devoted to the development of alternative anode materials with improved specific energy for replacing the graphite used in commercial Li-ion batteries. Metal-based composite oxides such as SnO_2 [1] and tin-based amorphous oxide [2] have been widely studied because of their high theoretical specific energy. Unfortunately, the reduction reaction of SnO with Li to yield metallic Sn and Li_2O causes a severe volume change of the electrode during the first cycling. Consequently, an irreversible conversion reaction occurs with significant loss of capacity.

The lithium reaction mechanism relies on the formation of Li–Sn alloy. Poizot et al. [3] reported that nano-sized transition metal oxides are be promising alternative anode materials with excellent electrochemical performance for lithium batteries. They also proposed a new mechanism for the Li reaction in which the reversible formation and de-formation of Li_2O occurs and is accompanied by the reduction and oxidation of metal nanosized particles, instead of a Li-metal alloying/de-alloying process. They suggested that the reactivity of the metal oxide particles is markedly determined by their particle size because Li_2O formed in reduction is electrochemically inactive and the reverse removal of lithium is thermodynamically difficult. Therefore, nanosized particles of metal oxide play an important role and enhance the electrochemical reactivity towards the formation/decomposition of Li_2O [3]. In fact, nanostructured materials have emerged as attractive alternatives to conventional materials by virtue of their prominent electronic and chemical properties [4].

Transition metal oxides can be prepared through various methods, such as liquid-control-precipitation [5], electron-beam evaporation [6], electrodeposition [7], chemical vapour deposition [8], the sol–gel route [9], and pulsed laser ablation [10]. These preparation methods are, however, very complicated and difficult to control.

The ultrasonic spray pyrolysis technique, by comparison, has several advantages such as simplicity and a low-cost alternative for the deposition of high-quality thin films of novel complex oxides [11]. Also, the method is applicable for the drying of

* Corresponding author. Tel.: +82 2 2220 0524; fax: +82 2 2282 7329.
E-mail address: yksun@hanyang.ac.kr (Y.-K. Sun).

0378-7753/$ – see front matter © 2007 Elsevier B.V. All rights reserved.
doi:10.1016/j.jpowsour.2007.04.087

colloids, direct control of microstructure and size of particles, and control of particle composition. When the precursor solution is atomized to form droplets and then pyrolyzed, the colloidal particles serve as seeds for nucleation. Thus, dense particles are easily formed.

In this study, nano-crystalline transition metal oxides (Co_3O_4, CuO, and NiO) powders are prepared via ultrasonic spray pyrolysis. Metal oxide particles with different crystallite sizes and morphologies are obtained at various calcination temperatures. The electrochemical performance of the nanosized transition metal oxides as anode materials for lithium ion batteries is investigated.

2. Experimental

Nano-crystalline metal oxide (Co_3O_4, CuO, and NiO) powders were synthesized by a spray pyrolysis method. Cobalt nitrate hexahydrate ($Co(NO_3)_2{\cdot}6H_2O$, Adrich), copper nitrate trihydrate ($Cu(NO_3)_2{\cdot}3H_2O$, Adrich) and nickel nitrate hexahydrate ($Ni(NO_3){\cdot}6H_2O$, Adrich) were used as the starting materials. Each metal salt was dissolved in distilled water. In each case, a solution containing the metal ions was added to a continuously agitated aqueous solution of citric acid. Citric acid ($C_6H_8O_7{\cdot}H_2O$, Duksan) was used as a polymeric agent for the reaction. The molar concentration of citric acid was fixed at 0.2 mol dm^{-3}.

Ammonium hydroxide was used to adjust and control the pH of the solution. The starting solution was atomized using an ultrasonic nebulizer with a resonant frequency of 1.7 MHz. The produced aerosol stream was carried into a vertical quartz reactor heated at 500 °C. The flow rate of air used as a carrier gas was 10 L min^{-1}. The resulting powders were heated at various temperatures between 300 and 900 °C at a heating rate of 1 °C min^{-1}.

Powder X-ray diffraction (XRD, Rint-2000, Rigaku) measurements using Cu Kα radiation were employed to identify the crystalline phase of the synthesized material. The particle morphology of the as-prepared and calcined powders was observed by means of scanning electron microscopy (SEM, JSM 6400, JEOL, Japan) and transmission electron microscopy (TEM, JEOL, 2010). Galvanostatic charge–discharge cycling was performed on a 2032-type coin type cell (Hohsen Co. Ltd., Japan). For fabrication of the working electrode, the selected transition metal oxide (Co_3O_4, CuO, and NiO) powder was mixed with Super-P carbon black as a conductive agent and poly vinylidene fluoride (PVDF) as a binder in a mass ratio of 80:10:10. The transition metal oxide (Co_3O_4, CuO, and NiO) and Super-P carbon black were first added to a solution of poly(vinyl difluoride) (PVDF) in *N*-methyl-2-pyrrolidone (NMP) to make a slurry of appropriate viscosity. The slurry was then casted on copper foil and dried at 110 °C overnight in a vacuum oven. Discs were then punched out of the foil. Li metal foil was used for the counter and reference electrodes. The electrolyte solution was 1 M $LiPF_6$ in a mixture of ethylene carbonate (EC) and diethyl carbonate (DEC) in a 1:1 volume ratio (CHEIL Industries Inc., Korea). The cell was assembled in an argon-filled dry box and tested at room temperature (30 °C). The cell was charged and discharged at a current density of 1 mA cm^{-2} with cut-off voltages of 0.01–3.0 V (versus Li/Li^+).

3. Results and discussion

The XRD patterns of the Co_3O_4, CuO, and NiO powders prepared by heating the respective precursor at different sintering temperatures are shown in Fig. 1. As the sintering temperature is increased, a sharpening of the peaks is observed, which indicates an increase in the degree of crystallization. The crystallite growth during the sintering process results from an increase in the average crystallite size because of a tendency for minimization of the interfacial surface energy [12]. The XRD patterns of Co_3O_4

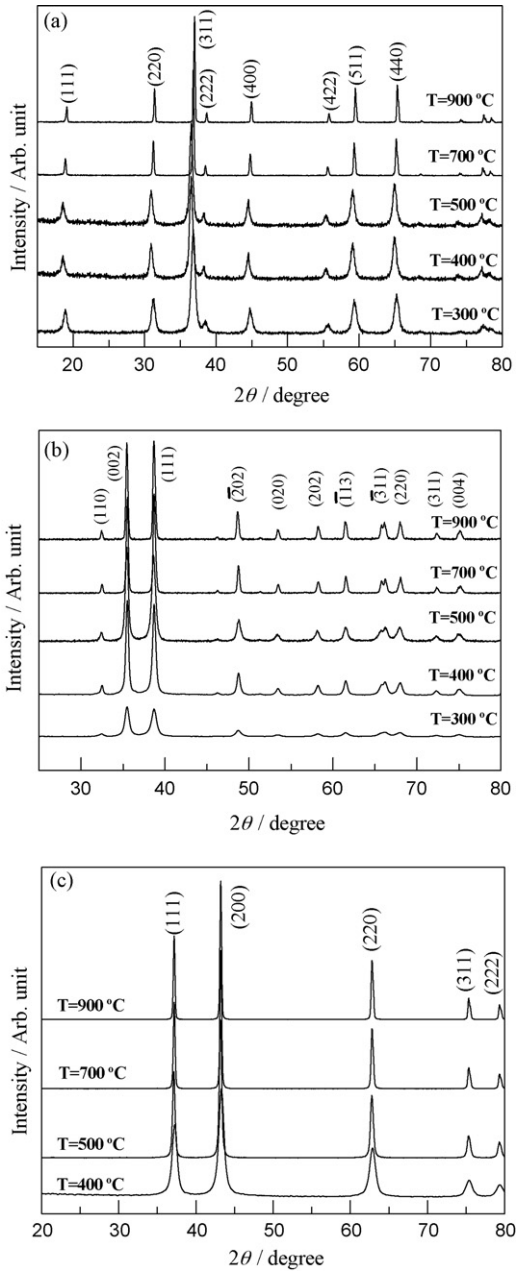

Fig. 1. X-ray diffraction (XRD) patterns of transition metal oxides powders sintered at different temperatures: (a) Co_3O_4, (b) CuO, (c) NiO.

in Fig. 1(a) can be indexed to a spinel-type cubic structure with a $F\bar{d}3m$ space group according to the JCPDS (No. 43-1003) and without detectable impurities. The XRD pattern of CuO calcined at 300 °C exhibits weak and broad peaks, see Fig. 1(b). As mentioned above, the peaks became more defined and shaper with increase in the calcination temperature. All peaks can be well indexed to the monoclinic lattice of CuO (JCPDS No. 05-0661). No significant impurities nor a second phase were observed, which indicates that high-purity CuO is obtained. The diffraction peaks of NiO powder can be indexed as the (1 1 1), (2 0 0), (2 2 0), (3 1 1) and (2 2 2) crystal planes of the crystalline cubic structure (JPDS No. 04-0835), see Fig. 1(c).

In order to investigate the effects of calcination temperature on the growth of crystallite size, the crystallite sizes of the prepared metal oxides were calculated from the major diffraction peaks of the corresponding Co_3O_4 (3 1 1), CuO (0 0 2), and NiO (2 0 0) using the Scherrer formula (Eq. (1)), i.e.,

$$D_c = \frac{K^*\lambda}{\theta_{1/2}} \cos\theta_B \quad (1)$$

where K^* is a constant (ca. 0.9); λ the X-ray wavelength (1.5418 Å); θ_B the Bragg angle; $\theta_{1/2}$ is the pure diffraction broadening of a peak at half-height, that is, broadening due to the crystallite dimensions. The evolution of the crystal size (D_c) of the metal oxides prepared at different calcination temperatures is shown in Fig. 2. The data show that the growth in crystallite size of each metal oxide has a strong relationship with the sintering temperature. The crystallite size of Co_3O_4 and NiO increase linearly until the calcination temperature reaches 700 °C. The variation in size for Co_3O_4 is from 20 to 62 nm over the temper-

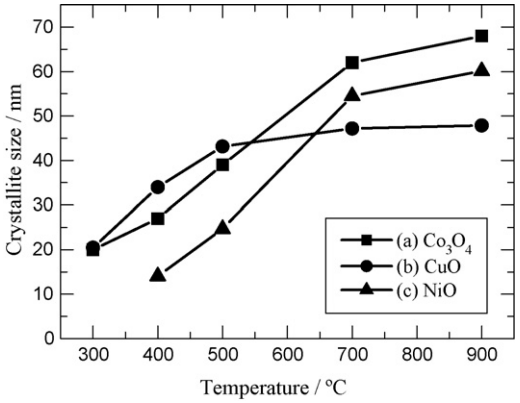

Fig. 2. Evolution of crystallite size of (a) Co_3O_4, (b) CuO and (c) NiO powders sintered at different temperatures.

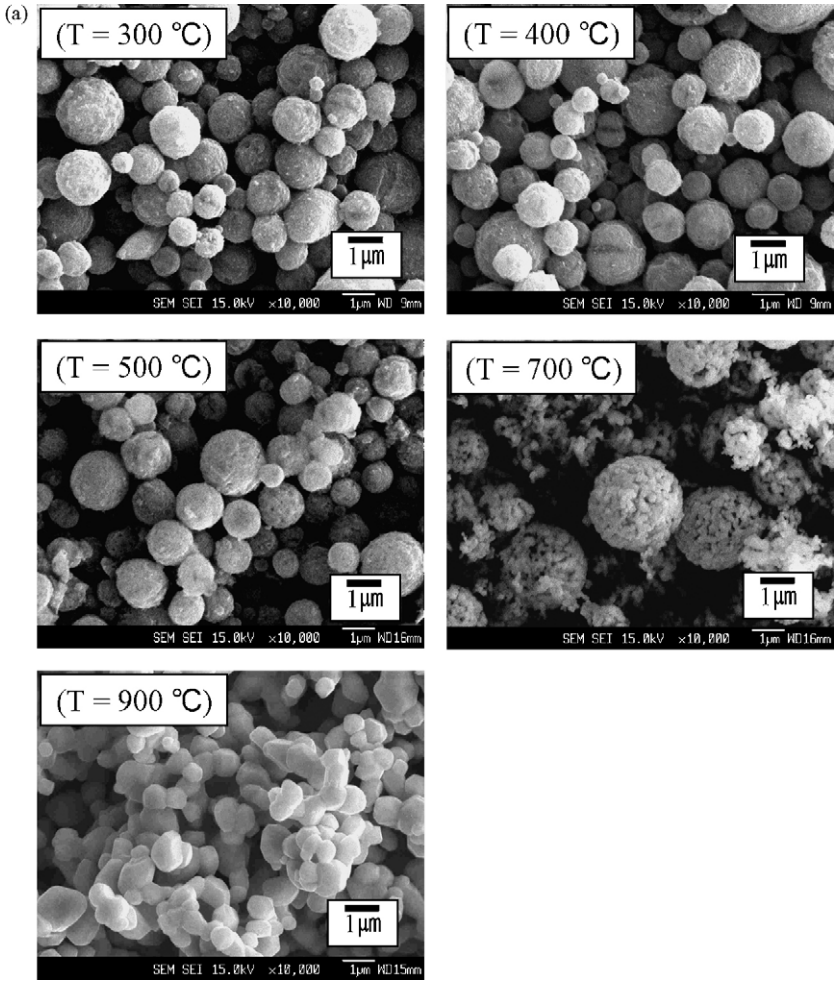

Fig. 3. Scanning electron microscopy (SEM) images of (a) Co_3O_4, (b) CuO and (c) NiO powders sintered at different calcination temperatures.

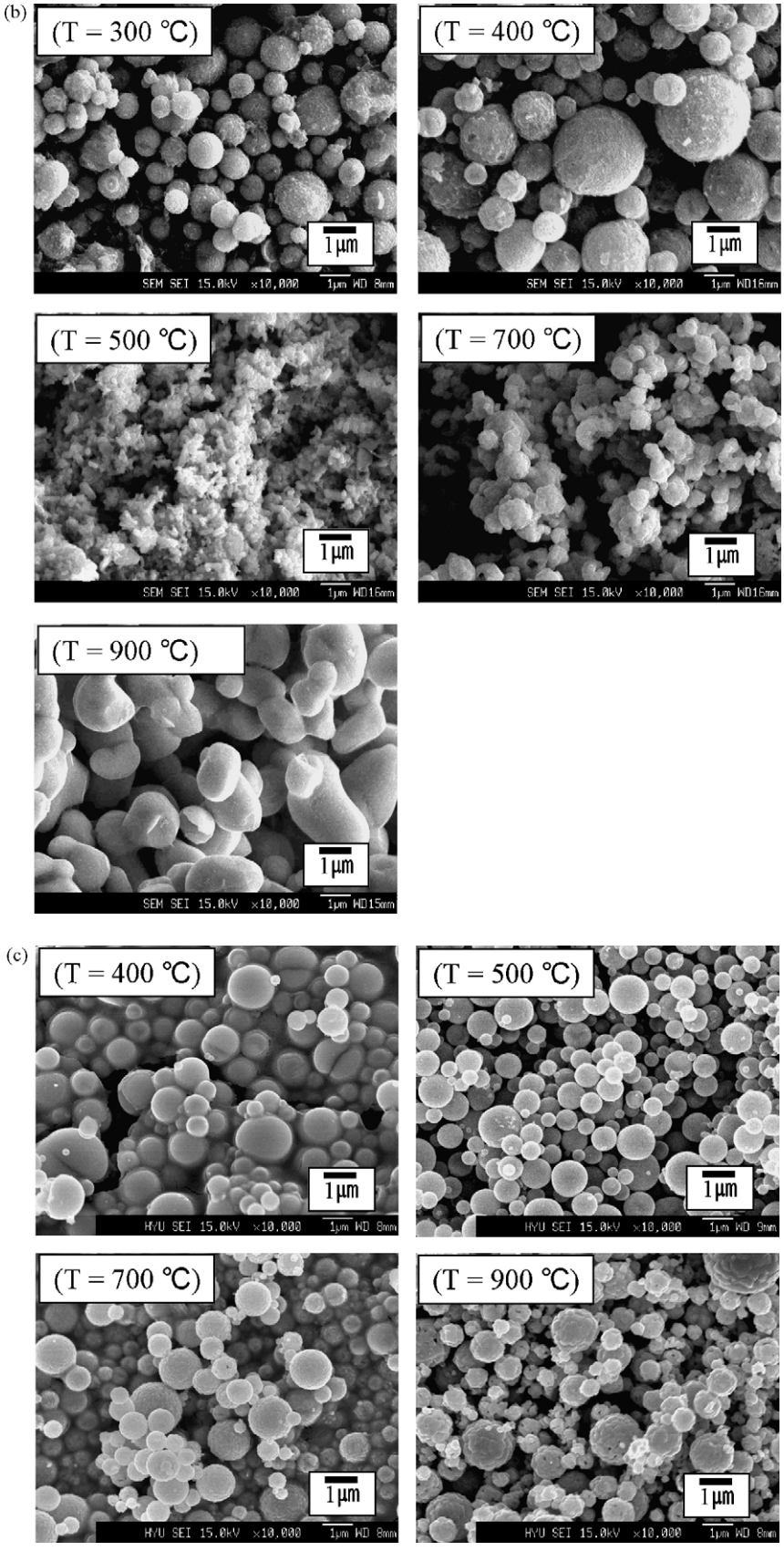

Fig. 3. (*Continued*).

ature range 300–700 °C. The size of NiO also increases linearly from 14 nm (400 °C) to 54 nm (700 °C). After 700 °C, the crystallite size of both metal oxides slightly increases to 69 nm (Co_3O_4) and 60 nm (NiO) at 900 °C. In case of CuO, the crystallite size increases until the calcination temperature reaches to 500 °C. At higher calcination temperatures (>500 °C), Cuo shows no significant change in crystallite size, which is 45 nm.

Scanning electron micrographs of the metal oxides obtained at different sintering temperatures also show a morphological changes. The micrograph of Co_3O_4 sintered at 300 °C in Fig. 3(a) shows that the oxide has a spherical particle shape with a 0.5–2 μm size distribution. Between 300 and 500 °C, no significant morphology change is observed and also the particle size remains at 0.5–2 μm. By contrast, the morphology of Co_3O_4 prepared at 700 °C starts to change in that the spherical particle consists of primary particles of sub-micrometer size that become scattered into small crystals. This morphological change becomes clearer for Co_3O_4 prepared at 900 °C. The spherical morphology of Co_3O_4 disappears and a new shape with a larger particle size is observed, as shown in Fig. 3(a). The CuO prepared at sintering temperatures of 300 and 400 °C exhibit similar morphological features (e.g., size and shape) to the Co_3O_4 powders, cf., Fig. 3(a and b). CuO prepared at 500 °C, however, shows a different morphological change, compared with Co_3O_4 prepared at the same temperature. The particles are fragmented into nano-crystalline particles. On increasing the calcination temperature to 700 °C, re-crystallization and agglomeration of the primary particles occurs. It is noteworthy to mention that the crystallite size of the CuO does increase after 500 °C. The NiO powders prepared at 400–900 °C have spherical shape with a mean diameter of 0.5–2 μm, see Fig. 3(c). It is interesting that as the sintering temperature is increased from 400 to 900 °C, the particle and agglomerate sizes remain unaltered. Between 400 and 700 °C, most of the particles have a smooth spherical shape. On the other hand, NiO prepared at 900 °C consists of particles with relatively coarse surfaces. These particles are composed of submicron-sized (approximately 200 nm) primary particles that form secondary agglomerates, as shown in Fig. 3(c).

In order to observe the detailed morphological difference of the metal oxides that exhibit drastic changes at specific calcination temperatures, TEM images of the metal oxides were taken. The TEM image of Co_3O_4 sintered at 700 °C is presented in Fig. 4(a). The nano-sized primary particles are well dispersed and formed agglomerates with a size of 300–500 nm. Based on the SEM image in Fig. 3(a), the agglomerate size of Co_3O_4 ($T = 700$ °C) is 300–600 nm, which is consistent with the observation from TEM results in Fig. 4(a). It is important to notice from the TEM image in Fig. 4(a) that Co_3O_4 prepared at 700 °C reveals the existence of empty inner spaces and that the nano-sized spherical particle consists of fine primary particles with a size ranging from 50 to 70 nm. Since CuO sintered at 500 °C exhibits a marched change in morphology (Fig. 3(b)), it was chosen for TEM analysis, which is presented in Fig. 4(b). The nano-sized CuO crystal has irregular morphology with a particle size of about 40–100 nm and the agglomerates grow in a random direction. It can be observed from Fig. 4(c) that NiO ($T = 500$ °C) forms hollow spherical particles with well dis-

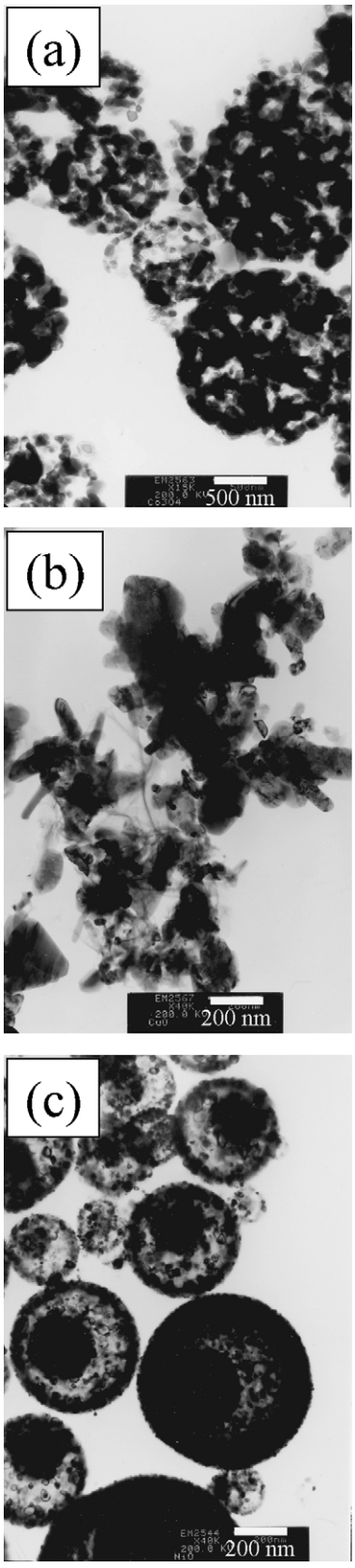

Fig. 4. Transmission electron microscopy (TEM) images of transition metal oxides: (a) Co_3O_4 sintered at 700 °C, (b) CuO sintered at 500 °C, (c) NiO sintered at 500 °C.

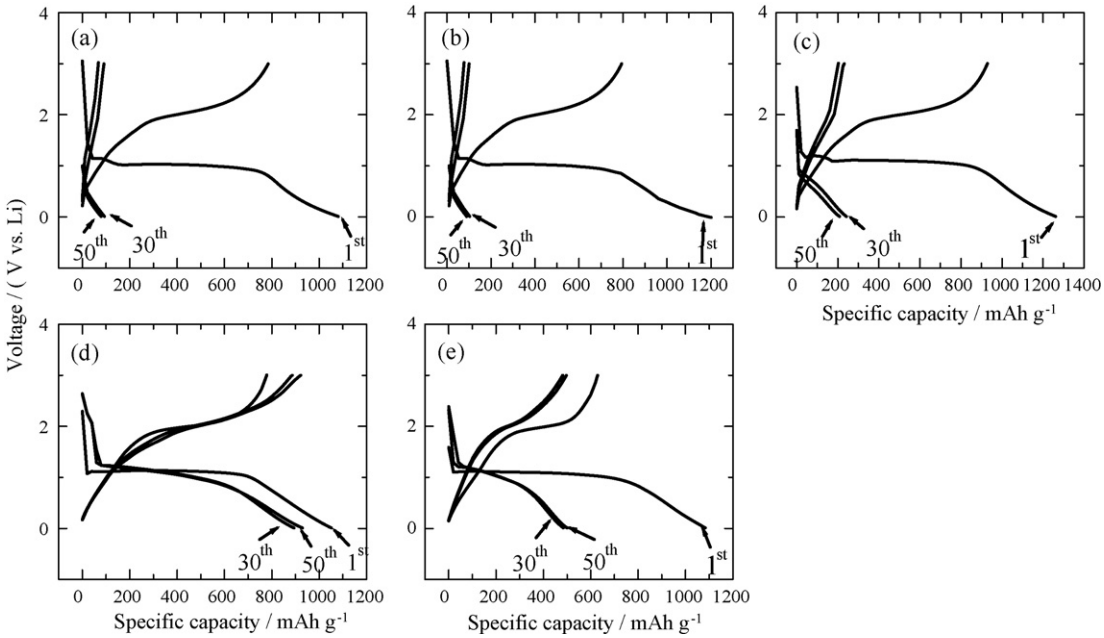

Fig. 5. Charge–discharge voltage profiles of electrodes made of Co_3O_4 prepared at calcination temperatures of (a) 300 °C, (b) 400 °C, (c) 500 °C, (d) 700 °C, (e) 900 °C.

persed nano-crystalline primary particles. The primary particles are fairly uniform with a mean diameter of ~20 nm scale, which is close to the estimated crystallite size by XRD analysis.

The electrochemical performances of the prepared metal oxides were evaluated by galvanostatic charge–discharge in the voltage range of 0.01–3 V versus Li/Li^+ at a constant current density of 1 mA cm^{-1}. The voltage profiles of MO/Li (MO = Co_3O_4, CuO, and NiO) cells at 1st, 30th and 50th cycles are given in Figs. 5–7, respectively. During the first discharge process, the potential profiles of all the Co_3O_4 electrodes have a long voltage plateau around 1.2 V and then showed a sloping voltage profile from 1.2 V to the cut-off voltage of 0.01 V, as shown in Fig. 5. The Co_3O_4 electrodes (T = 300, 400 and 500 °C) prepared at temperatures below 500 °C display fast capacity fading with a large irreversible capacity loss, whereas the Co_3O_4 prepared at 700 °C delivers the highest reversible capacity (925 mAh g^{-1}) with good capacity retention. The irreversible capacity occurring during the first cycle is probably

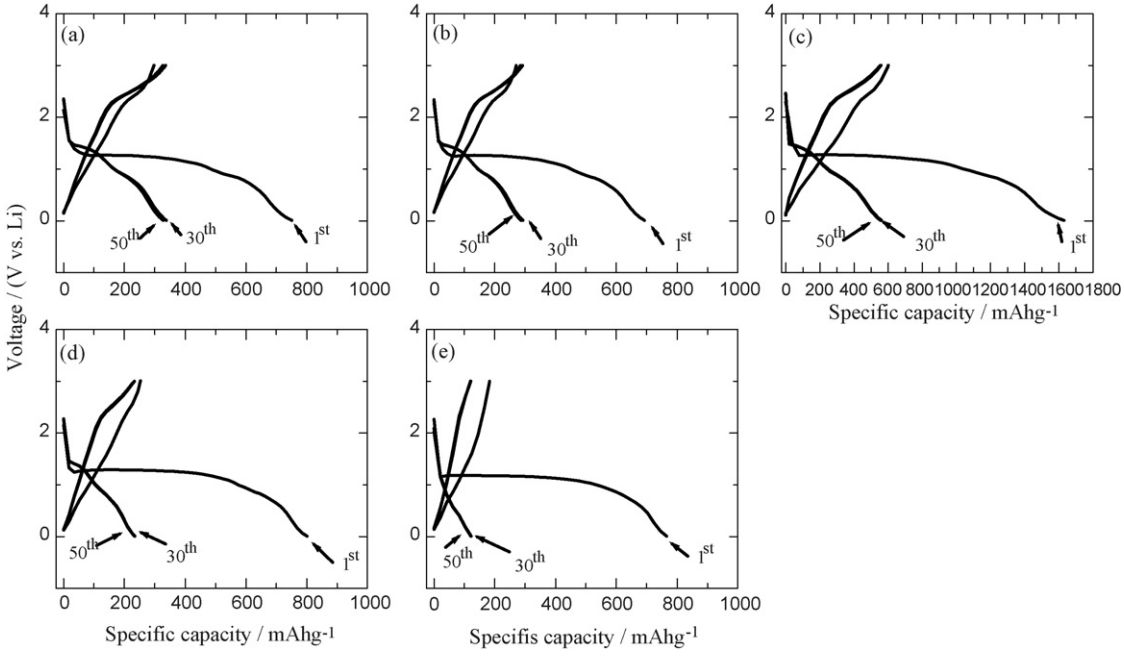

Fig. 6. Charge–discharge voltage profiles of electrodes made of CuO prepared at calcination temperatures of: (a) 300 °C, (b) 400 °C, (c) 500 °C, (d) 700 °C, (e) 900 °C.

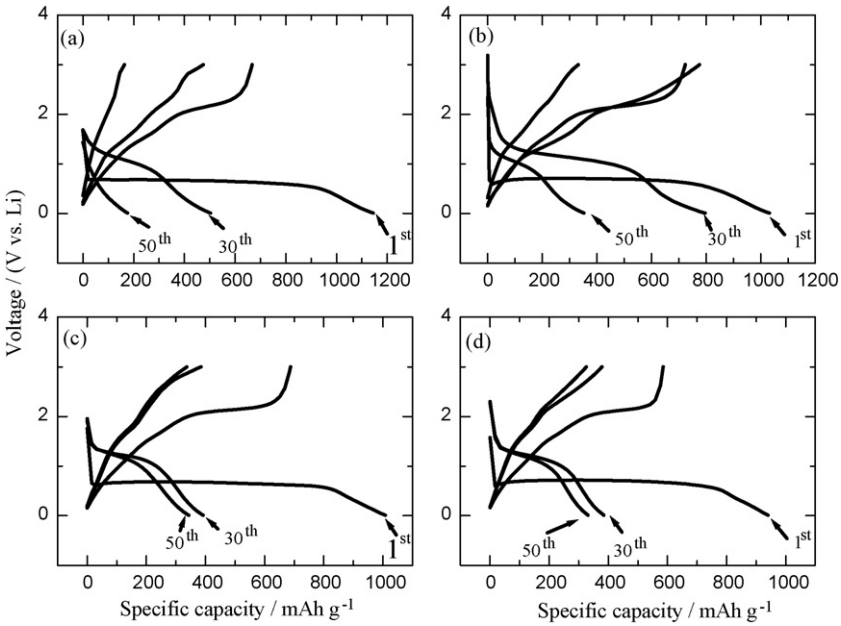

Fig. 7. Charge–discharge voltage profiles of electrodes made of NiO prepared at calcination temperature of (a) 400 °C, (b) 500 °C, (c) 700 °C, (d) 900 °C.

related to the formation/deformation of Li_2O as well as typical solid electrolyte interface (SEI) film formation [3,13]. Lithium reacts with Co_3O_4 during the first discharge and forms Li_2O and metal (Co), as mentioned earlier. Li_2O is known to be electrochemically inactive and the incomplete decomposition of Li_2O is responsible for the large irreversible capacity loss during cycling. Poizot et al. [3] proposed that reducing the particle size of the metal oxide to the nano-level would affect the electrochemical reactivity since the chemical and physical properties of nano-sized materials can be different from their bulk (intrinsic) properties. The Co_3O_4 electrode (900 °C), however, shows a decrease of reversible capacity.

The charge–discharge curves of the CuO electrodes at prepared at different calcination temperatures are presented in Fig. 6. The overall voltage profiles are similar to those of the Co_3O_4 electrode. During the first discharge process, the CuO electrode also exhibits a similar long voltage plateau around 1.25 V followed by a sloping voltage profile to 0.01 V that is due to lithium uptake by the metal oxide structure. All CuO electrodes in Fig. 6 (except that prepared at 500 °C) deliver 700–800 mAh g^{-1} of discharge capacity on the first cycle with more than 400 mAh g^{-1} of irreversible capacity. By contrast, the CuO electrode prepared at 500 °C yields 1630 mAh g^{-1} on the first discharge capacity, as shown in Fig. 6(c). The amount of lithium that is reacted on the first discharge is estimated to be 2.47 of Li per Cu for CuO prepared at 500 °C. For the first charge process, 600 mAh g^{-1} is obtained, which implies that only 0.89 Li is reversibly extracted from lithiated CuO structure. During subsequent cycles, a large irreversible capacity is not observed and the discharge capacities of the 30th and 50th cycles are about 596 and 592 mAh g^{-1}, respectively.

Charge–discharge curves of the NiO electrodes are given in Fig. 7. In the first discharge process, the potential of all electrodes rapidly falls and reaches a long voltage plateau around 0.65 V followed by a sloping voltage profile similar to that of the CuO electrodes. The first discharge capacity of NiO electrodes prepared at different temperatures varies from 960 to 1150 mAh g^{-1}, i.e., much higher than the theoretical capacity (718 mAh g^{-1}) for reduction from NiO to Ni. The first charge process exhibits a higher and sloping voltage profile with large irreversible capacity. The explanation for the irreversible capacity of the all NiO electrode could be analogous to that for Co_3O_4. The irreversible capacity loss between the first discharge and charge is attributed to the incomplete decomposition of both of the SEI and Li_2O [3,13,14]. In the 30th, 50th discharge process, the voltage plateau appears at higher voltage of 1.25 V, which is higher than that of the first discharge (about 0.66 V). The first discharge capacity of the NiO ($T = 500$ °C) electrode reaches 1031 mAh g^{-1}.

Discharge capacity versus cycle number plots for MO/Li (Co_3O_4, CuO, and NiO) electrodes prepared at different calcination temperatures are given in Fig. 8. It can be clearly observed from Fig. 8(a) that Co_3O_4 electrodes prepared at low temperature (300 °C $\leq T \leq$ 500 °C) display a fast capacity fading, whereas the Co_3O_4 electrodes prepared at higher temperature ($T = 700$ and 900 °C) show relatively good capacity retention. In particular, the Co_3O_4 ($T = 700$ °C) electrode exhibits excellent capacity retention, indeed there is a slight increase in capacity as cycling proceeds. It is proposed that the electrochemical properties of metal oxides, such as capacity retention and rate capability, are strongly influenced by particle size, grains and the particle size of the precursor [2,3,13,15]. In addition, the formation of the SEI layer may affect capacity retention. If the SEI layer is too thick, it will hinder the Co_3O_4 particle reactivity towards lithium and result in capacity fading [16]. It is important to recall from Fig. 3(a) that Co_3O_4 ($T = 700$ °C) particles consist of nano-sized primary particles with a different morphology, compared with the other electrodes. As shown in Fig. 8(a), Co_3O_4 ($T = 700$ °C)

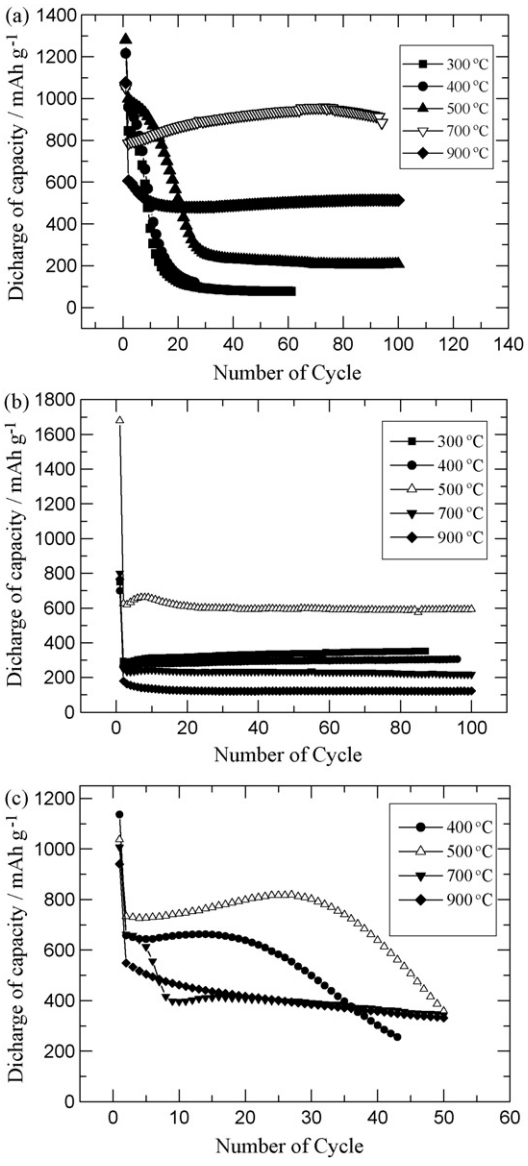

Fig. 8. Discharge capacity vs. number of cycle of MO/Li cells (a) Co_3O_4, (b) CuO, and (c) NiO prepared at different calcination temperature and at a current density of 1 mA cm^{-2}.

gives a capacity retention of 900 mAh g^{-1} at 100 cycles, which suggests that there is an optimum sintering temperature and particle size for Co_3O_4 anode material that produces excellent capacity retention.

The discharge capacity versus cycle number for CuO electrodes prepared at different sintering temperatures is presented in Fig. 8(b). Among the electrodes, the CuO (T = 500 °C) electrode provides much higher reversible capacities and better cycling performance than the other electrodes. There is no appreciable change in the discharge capacity even after 100 cycles. This result suggests that no observable structural degradation of the nano-sized CuO takes place during repeated cycling. As shown in Fig. 8(c), all NiO electrodes commonly experience a gradual decrease of discharge capacity with cycling. The capacity of NiO prepared at 400 and 500 °C initially gave higher capacity than NiO prepared at 700 and 900 °C. The capacity fade of NiO (T = 400 and 500 °C) is faster than of NiO (T = 700 and 900 °C).

4. Conclusions

Nano-crystalline metal oxides (Co_3O_4, CuO, and NiO) have been synthesized via an ultrasonic spray pyrolysis method. The effect of the final calcination temperature on the morphology, crystallinity size and electrochemical properties of the metal oxides (Co_3O_4, CuO, and NiO) has been investigated. From XRD analysis, it is found that the crystallite size of the metal oxides varies with the calcination temperature, namely, the crystallite size increases linearly with increase in temperature until a constant size is achieved. The morphology of metal oxides is also strongly influenced by the final calcination temperature. The morphological difference induced by the final calcination temperature also affects the electrochemical performance of the metal oxides. Evaluation of the electrochemical performance in combination with observation of the morphology of metal oxides by SEM and TEM analysis suggests that there is an optimum calcination temperature for each metal oxide. It is found that the optimum calcination temperature is 700, 500 and 500 °C for Co_3O_4, CuO and NiO, respectively.

Acknowledgement

The research was supported by a University IT Research Center Project.

References

[1] I.A. Courtney, J.R. Dahn, J. Electrochem. Soc. 144 (1997) 2045.
[2] Y. Idota, T. Kubota, A. Matsufuji, Y. Maekawa, T. Miyasaka, Science 276 (1997) 1395.
[3] P. Poizot, S. Laruelle, S. Grugeon, L. Dupont, J.-M. Tarascon, Nature 407 (2000) 496.
[4] J. Schoonman, Solid State Ionics 135 (2000) 5.
[5] Y. Li, Y. He, L. Li, Chem. J. Chin. Univ. 20 (1990) 519.
[6] T. Seike, J. Nagai, Sol. Energy Mater. 22 (1991) 107.
[7] C.N.P.da. Fonseca, M.-A.de. Paoli, A. Gorenstein, Adv. Mater. 3 (1991) 553.
[8] T. Maruyama, S.J. Arai, J. Electrochem. Soc. 143 (1996) 1383.
[9] F. Svegl, B. Orel, I.G. Svegl, V. Kaucic, Electrochim. Acta 45 (2000) 4359.
[10] Y. Wang, Q.-Z. Qin, J. Electrochem. Soc. 149 (2002) A873.
[11] W.W. Xu, R. Kershaw, K. Dwight, A. Wold, Mater. Res. Bull. 25 (1990) 1385.
[12] W.D. Kingery, H.K. Bowen, D.R. Uhlmann, Introduction to Ceramics, John Wiley and Sons, New York, 1976, p. 522.
[13] A. Debart, L. Dupont, P. Poizot, J.-B. Leriche, J.M. Tarascon, J. Electrochem. Soc. 148 (2001) A1266.
[14] X.H. Huang, J.P. Tu, B. Zhang, Y. Li, Y.F. Yuan, H.M. Wu, J. Power Sources 161 (2006) 541.
[15] N. Li, C.R. Martin, B. Scrosati, J. Power Sources 97–98 (2001) 240.
[16] Z. Yuan, F. Huang, C. Feng, J. Sun, Y. Zhou, Mater. Chem. Phys. 79 (2003) 1.